STABLE WALKING OF A 7-DOF BIPED ROBOT

F. Plestan* , J.W. Grizzle+, E.R. Westervelt+, G. Abba×

Abstract

The primary goal of this paper is to demonstrate a means to prove asymptotically stable walking in a planar, under actuated, five-link biped robot model. The analysis assumes a rigid contact model when the swing leg impacts the ground and an instantaneous double-support phase. The specific robot model analyzed corresponds to a prototype under development by the CNRS in France. The viability of the theoretically motivated control law is demonstrated on a detailed simulator for the prototype which includes torque limits and a compliant model of the ground, and thus a non-instantaneous double support phase.

Keywords. Biped robot, stable walking, Poincaré's sections, rigid and compliant grounds

I. Introduction

This paper develops a provably, asymptotically stabilizing controller for the walking motion of a prototype, five-link, planar biped robot consisting of a torso and two legs with knees but no feet; see Figure 1. The prototype, named RABBIT[1], has four independent actuators: the axis between the torso and each thigh is actuated as is the axis of each knee. The actuators have been sized so that robot is capable of generating motions of at least 5km/h when walking and 12km/h when running. These speeds compare well with the capabilities of humans [6]. Many of the technical considerations that went into the design of the robot are summarized in [6]. The principal motivations for constructing the prototype were to study modeling (especially hybrid mechanical systems and compliant contact models), determination of optimal trajectories, limit cycles, stabilization of trajectories and the transition between walking and running [28].

The prototype is limited to motion in the saggital plane by means of a radial bar. While the end of the robot's legs are fitted with wheels, these are provided so that radial movements of the contact points between the robot's leg and the floor are completely free; no mobility exists between the legs and the "feet" in the sagittal plane. The radius of the circular path imposed by the bar is approximately 3 m. The design of stabilizing controllers for the lateral motion of a walking robot has been addressed in [18], where it is shown that stability can be achieved by actively adjusting the lateral distance

* **Corresponding author.** IRCCyN, Ecole Centrale de Nantes, UMR CNRS 6597, BP 92101, 1 rue de la Noe, 44321 Nantes cedex 03, France, Franck.Plestan@irccyn.ec-nantes.fr

+ Control Systems Laboratory, Electrical Engineering and Computer Science Department, University of Michigan, Ann Arbor, MI 48109-2122, USA, {grizzle,ewesterv}@umich.edu

× LGIPM, Université de Metz, IUT de Thionville, Espace Cormontaigne, 57970 Yutz, France, abba@iut.univ-metz.fr

[1] The RABBIT prototype has been developed by the French Project *Commande de Robots à Pattes* of the *CNRS - GdR Automatique*.

between the feet; this issue is not studied here. Section II develops the dynamical model of the robot and specifies all of the mechanical parameters. A rigid model is used for the contact between the swing leg and ground and the double support phase in assumed to be instantaneous. The contact between the support leg and the ground is modeled as a pivot, so, when walking on a rigid surface, the model has five degrees of freedom. Section III develops the controller. The work presented here is a natural continuation of [11], [12] where the asymptotic stability of the walking motion of a robot with a torso, two legs and no knees was fully proved. *The structure of the controller is motivated by the desire to render as tractable as possible the task of rigorously establishing the asymptotic stability of walking motions.* The principal idea is to design the controller so that the image of the Poincaré map has dimension one, which greatly simplifies the stability analysis problem. The controller's performance is first evaluated by simulation in Section IV, under the hypotheses of a rigid contact model, an instantaneous double support phase, and no slipping of the support leg. The simulations indicate that the controller induces an asymptotically stable walking motion of 0.75 m/s, with peak torques of 105 Nm. The required torques are well within the capabilities of the prototype. The actual stability of the induced walking motion is then proven in Section V under the above hypotheses.

As a final step before implementing the controller on the prototype, the controller's performance is evaluated in Section VI on a more detailed simulator developed by the French Project *Commande de Robots à Pattes* [28]. The main novelty of the detailed simulator is the inclusion of a nonlinear, compliant model of the contact between the robot's limbs and the ground [14], [20], [5] and a dynamic friction model [4], [19], [23]. The detailed simulator thus exercises all seven of the robot's degrees of freedom (the angles of the five links plus the Cartesian coordinates of the hips), and thus serves as an independent check of the validity of the key hypotheses made in the mathematical derivation of the controller; in particular, the contact points of the limbs may slip and/or rebound, and the double support phase is not instantaneous. The controller's performance on the more complete model is shown to be very similar to that obtained under the idealized hypotheses of Section IV.

II. Robot model

The robot is modeled as a planar biped. It consists of a torso, hips, and two legs with knees, but no ankles (see Figure 1). It thus has 7 degrees of freedom (the five joint angles plus the Cartesian

coordinates of the hips, for example). A torque is applied between each leg and the torso, and a torque is applied at each knee. It is assumed that the walking cycle takes place in the sagittal plane and consists of successive phases of single support.

The complete model of the biped robot consists of two parts: the differential equations describing the dynamics of the robot during the swing phase (these equations are derived using the method of Lagrange [25]), and an impulse model of the contact event (the impact between the swing leg and the ground is modeled as a contact between two rigid bodies [15]). The contact between the stance leg and the ground is modeled as a pivot. As in [11], [12], the complete model can be expressed as a nonlinear system with impulse effects [27].

A. Swing phase model

The dynamic model of the robot between successive impacts is derived from the Lagrange formalism

$$D(q)\cdot\ddot{q}+C(q,\dot{q})\cdot\dot{q}+G(q) \;=\; B\cdot u \tag{1}$$

with $q=(q_{31},q_{41},q_{32},q_{42},q_1)'$ (see Figure 2) and $u=(u_1,u_2,u_3,u_4)'$ (see Figures 4 and 5). The torques u_1, u_2, u_3, and u_4 are applied between the torso and the stance leg, the torso and the swing leg, at the knee of the stance leg and at the knee of the swing leg, respectively. The model can be written in state space form by defining

$$\dot{x}:=\frac{d}{dt}\begin{bmatrix} q \\ \omega \end{bmatrix}=\begin{bmatrix} \overset{\omega}{} \\ D^{-1}(q)\cdot(-C(q,\omega)\cdot\omega-G(q)-B\cdot u) \end{bmatrix} \;=:\; f(x)+g(x)\cdot u \tag{2}$$

where $\omega:=\dot{q}$, and $x:=(q',\omega')'$. The state space of the model will be restricted to physically reasonable values of q for walking. To define these bounds, it is convenient to introduce the coordinates $(p_{31},p_{41},p_{32},p_{42})$ (see Figure 3) where

$$\begin{bmatrix} p_{31} \\ p_{41} \\ p_{32} \\ p_{42} \end{bmatrix} \;=\; \begin{bmatrix} \frac{1}{2}(q_{31}+q_{41}) \\ \pi+q_{41}-q_{31} \\ \frac{1}{2}(q_{32}+q_{42}) \\ \pi+q_{42}-q_{32} \end{bmatrix}. \tag{3}$$

Note that, for the computation of (3), it is assumed that the two legs of the biped robot have the same length, and the tibia and the femur have also the same length (it is the case of the prototype RABBIT). The variable p_{31} (resp. p_{32}) is the angle between the vertical axis and a "virtual" leg joining the hips to the foot of the stance leg (resp. the swing leg) and the variable p_{41} (resp. p_{42}) is the

relative angle of the stance leg (resp. swing leg) knee. The state space for the system will be taken as $\mathcal{X} := \{(q', \omega')' \mid q \in M,\ \omega \in I\!R^5\}$, where $M = \{q \mid -\frac{\pi}{2} < q_1 < \frac{\pi}{2},\ \frac{3\pi}{4} < p_{31} < \frac{5\pi}{4},\ 0 < p_{41} < \pi,\ \frac{3\pi}{4} < p_{32} < \frac{5\pi}{4},\ 0 < p_{42} < \pi\}$. With this choice of M, the robot's torso and support leg are never below the walking surface, which is taken as $\{(q, \omega) \in \mathcal{X} | z_1 = 0\}$, the set of points where the height of the end of the support leg is zero.

B. Impact model

An impact occurs when the swing leg touches the walking surface, also called the ground. The impact between the swing leg and the ground is modeled as a contact between two rigid bodies. The development of the impact model requires the full seven degrees of freedom of the robot. Let us add Cartesian coordinates (x_H, z_H) to the hips. One then obtains the following extended model

$$D_e(q_e) \cdot \ddot{q}_e + C_e(q_e, \dot{q}_e) \cdot \dot{q}_e + G_e(q_e) \quad = \quad B_e \cdot u + \delta F_{ext} \tag{4}$$

with $q_e = (q_{31}, q_{41}, q_{32}, q_{42}, q_1, x_H, z_H)'$. δF_{ext} represents the external forces acting on the robot at the contact point. The basic hypotheses are

1. the contact of the swing leg with the ground results in no rebound and no slipping of the swing leg;
2. at the moment of impact, the stance leg lifts from the ground without interaction;
3. the impact is instantaneous;
4. the external forces during the impact can be represented by impulses;
5. the impulsive forces may result in an instantaneous change in the velocities, but there is no instantaneous change in the positions; and
6. the torques supplied by the actuators are not impulsional.

From these hypotheses, the angular momentum is conserved. One deduces

$$D_e(\dot{q}_e^+ - \dot{q}_e^-) \quad = \quad F_{ext} \tag{5}$$

where F_{ext} is the result of the contact impulse forces. $\dot{q}_e^+$ (resp. $\dot{q}_e^-$) is the velocity just after (resp. before) impact. An additional set of two equations is obtained by supposing that the stance leg does not rebound nor slip at impact. Then, from the condition that the swing leg does not rebound nor slip at impact, one obtains

$$\frac{d}{dt} E(q_e) \quad = \quad \frac{\partial E}{\partial q_e} \cdot \dot{q}_e^+ = 0 \tag{6}$$

with $E(q_e) = (x_2, z_2)'$ the Cartesian coordinates of the end of the swing leg. The result of solving (5) and (6) yields an expression[2] for $\dot{q}_e^+$ in term of $\dot{q}_e^-$. The final result is an expression for $x^+ := (q^+, \omega^+)$ (state value just after the impact) in terms of $x^- := (q^-, \omega^-)$ (state value just before the impact), which is expressed as

$$x^+ \quad = \quad \Delta(x^-). \tag{7}$$

C. Nonlinear system with impulse effects

The overall biped robot model can be expressed as a nonlinear system with impulse effects [27]

$$\begin{array}{rcll} \dot{x} & = & f(x) + g(x) \cdot u & x^- \notin S \\ x^+ & = & \Delta(x^-) & x^- \in S, \end{array} \tag{8}$$

where,

$$S := \{(q, \omega) \in \mathcal{X} | z_2 = 0, L_{f+gu} z_2 < 0\}. \tag{9}$$

Solutions are taken to be right continuous (see [12] for details). With this convention, as long as the robot is initialized in $\mathcal{X}$ with the swing leg on or above the walking surface, all valid solutions of the model result in the robot remaining on or above the walking surface.

III. Feedback Controller Design

This section develops the extension of the controller of [11], [12] for the 5 link biped with knees. The fundamental idea is to encode walking in terms of a set of "posture conditions", which are in turn expressed as "holonomic constraints" on the position variables. These "constraints" are then used to construct outputs of the mechanical model and are "imposed" on the robot via feedback control. The controller is designed on the basis of the assumptions made in Section II, namely that the impact model is rigid and the double support phase is instantaneous. These hypotheses will be re-visited in Section VI.

A. Output definition

In human walking, one observes that the torso is maintained at a nearly vertical angle, the hips remain roughly centered between the feet and at a nearly constant height above the walking surface, and the end of the swing leg traces an approximately parabolic trajectory. In addition, the knees are

[2]The solvability of the equations is easily verified; see [12].

never hyper-extended (as opposed to a bird) and only slightly flexed (as opposed to a monkey). These observations have been used to build a set of control objectives through the following output functions:

$$\begin{array}{rcl} y_1 &=& k_1 \cdot (q_1 - q_{1d}) \\ y_2 &=& k_2 \cdot (d_1 + d_2) \\ y_3 &=& k_3 \cdot (z_H - z_{Hd}(d_1)) \\ y_4 &=& k_4 \cdot (z_2 - z_{2d}(d_1)). \end{array} \tag{10}$$

In the above, the coordinates of the hips, (x_H, z_H), and the end of the swing leg, (x_2, z_2), are expressed in the coordinate frame of the foot of the stance leg, (x_1, z_1) (see Figure 2):

$$\begin{array}{rcl} x_1 &=& 0 \\ z_1 &=& 0 \\ x_H &=& L_3 \cdot \sin(q_{31}) + L_4 \cdot \sin(q_{41}) \\ z_H &=& -L_3 \cdot \cos(q_{31}) - L_4 \cdot \cos(q_{41}) \\ x_2 &=& x_H - L_3 \cdot \sin(q_{32}) - L_4 \cdot \sin(q_{42}) \\ z_2 &=& z_H + L_3 \cdot \cos(q_{32}) + L_4 \cdot \cos(q_{42}) \\ d_1 &=& x_H - x_1 = L_3 \cdot \sin(q_{31}) + L_4 \cdot \sin(q_{41}) \\ d_2 &=& x_H - x_2 = L_3 \cdot \sin(q_{32}) + L_4 \cdot \sin(q_{42}). \end{array} \tag{11}$$

The output y_1 is chosen to maintain the angle of the torso at a desired constant value, say q_{1d}. The output y_2 ensures the advancement of the hips while the swing leg goes from behind the stance leg to in front of it (see Figure 3 for the definition of d_1 and d_2). The output y_3 controls the hip height in such a way that the hips can rise and fall by a small amount in a natural way. The desired trajectory z_{Hd} of the hips is defined as a second order polynomial of d_1 such that $d_1 \in [-\text{sld}/2, \text{sld}/2]$, where sld is the desired step length, $z_{H\text{MAX}}$ (resp. $z_{H\text{MIN}}$) is the maximum (resp. minimum) desired value of z_H over a step and

$$z_{Hd}(-\text{sld}/2) = z_{H\text{MIN}}, \qquad z_{Hd}(0) = z_{H\text{MAX}}, \qquad z_{Hd}(\text{sld}/2) = z_{H\text{MIN}}. \tag{12}$$

The output y_4 controls the trajectory of the end of the swing leg; the desired trajectory z_{2d} is defined as a second order polynomial of d_1 such that $d_1 \in [-\text{sld}/2, \text{sld}/2]$, where $z_{2\text{MAX}}$ is the maximum desired value of z_2 over a step and

$$z_{2d}(-\text{sld}/2) = 0, \qquad z_{2d}(0) = z_{2\text{MAX}}, \qquad z_{2d}(\text{sld}/2) = 0. \tag{13}$$

The gains k_1, k_2, k_3 and k_4 are constant values to be chosen later. Thus, with the same notation as in (10), the output vector reads as

$$y = h(q) := \begin{bmatrix} h_1(q) \\ h_2(q) \\ h_3(q) \\ h_4(q) \end{bmatrix} = \begin{bmatrix} k_1 \cdot (q_1 - q_{1d}) \\ k_2 \cdot (d_1(q) + d_2(q)) \\ k_3 \cdot (z_H(q) - z_{Hd}(d_1(q))) \\ k_4 \cdot (z_2(q) - z_{2d}(d_1(q))) \end{bmatrix}. \tag{14}$$

B. Controller synthesis

The control objective is to drive the outputs (14) to zero. Since the outputs (14) only depend on the generalized positions, q, and the dynamic model (2) is second order, the relative degree of each output component is either two or infinite. Using standard Lie derivative notation [16], [25], direct calculation yields

$$\ddot{y} \;=\; L_f^2 h(x) + L_g L_f h(x) \cdot u. \tag{15}$$

For the moment, it is supposed that the matrix $L_g L_f h$ is invertible on the region of interest. This will be confirmed later in the paper. The method of computed torque (or inverse dynamics) can then be used to define

$$v := L_f^2 h + L_g L_f h \cdot u, \tag{16}$$

resulting in four double integrators

$$\ddot{y}_i \;=\; v_i, \quad i = 1 \text{ to } 4. \tag{17}$$

One possible approach to control design would be to design asymptotically stabilizing controllers, such as $v_i = k_{i1} y_i + k_{i2} \dot{y}_i$, for the double integrators (17). In general, when such a feedback is applied to the full hybrid model (8), it is no longer able to drive the outputs (14) asymptotically to zero due to the impulsive effects of the impacts. A general means of trying to "overcome" this can be observed in the literature: for experimental as well as simulation based studies, the feedback gains appear to be universally chosen sufficiently large so that the time constant for driving the outputs to zero is much less than the time interval of a single step. A biological basis for doing this is much more difficult to establish because the experiments are not easy to do well. Nevertheless, the evidence suggests that if a perturbation is deliberately introduced in a human's gait [7], [8], the subject's gait will recover to its original state in just a few cycles.

The use of high-gain control can be made to work quite well in simulation. The difficulty comes in mathematically analyzing the existence and stability of periodic orbits induced by the controller. Since we are dealing with periodic orbits, Poincaré's method is the appropriate tool. However, to apply it one must compute the induced discrete-time dynamics from a hyper-surface transversal to the orbit back to the hyper-surface [13], [21]. The induced discrete-time dynamics is called the Poincaré map. In the case of the model (8), the hyper-surface has dimension nine and the computation of

the Poincaré map is impractical. The key idea established in [12] is that for a mechanical system with N-degrees of freedom and m-independent inputs, the feedback control design can be carried out in a way that greatly simplifies the stability analysis problem: the dimension of the image of the Poincaré map can be reduced from $2N-1$ to $N-m$. For the biped considered here, this results in a *one-dimensional* analysis problem. The Poincaré map for this one-dimensional problem must still be computed numerically. The main points are that its numerical computation is very easy and it leads to *conclusive existence and stability properties* for periodic orbits. The feedback design proceeds as follows. Define a continuous[3] feedback $v = v(y, \dot{y})$ on (15) so that each of the four double integrators $\ddot{y}_i = v_i$ is (globally) finite-time stabilized. The feedback functions used here come from [2]:

$$v \;\; = \Psi(y,\dot{y}) \;\; := \tfrac{1}{\epsilon^2} \cdot \begin{bmatrix} \psi_1(y_1, \epsilon \cdot \dot{y}_1) \\ \psi_2(y_2, \epsilon \cdot \dot{y}_2) \\ \psi_3(y_3, \epsilon \cdot \dot{y}_3) \\ \psi_4(y_4, \epsilon \cdot \dot{y}_4) \end{bmatrix}. \tag{18}$$

Each function $\psi_i(y_i, \epsilon \cdot \dot{y}_i)$ ($i = 1$ to 4) is defined as

$$\psi_i(y_i, \epsilon \cdot \dot{y}_i) \;\; := \;\; -\text{sign}(\epsilon \cdot \dot{y}_i) \cdot |\epsilon \cdot \dot{y}_i|^{\alpha} - \text{sign}(\phi_i(y_i, \epsilon \cdot \dot{y}_i)) \cdot |\phi_i(y_i, \epsilon \cdot \dot{y}_i)|^{\frac{\alpha}{2-\alpha}} \tag{19}$$

with $0 < \alpha < 1$ and

$$\phi_i(y_i, \epsilon \cdot \dot{y}_i) \;\; = \;\; y_i + \tfrac{1}{2-\alpha} \text{sign}(\epsilon \cdot \dot{y}_i) \cdot |\epsilon \cdot \dot{y}_i|^{2-\alpha}. \tag{20}$$

The real parameter $\epsilon > 0$ allows the settling time of the controllers to be adjusted. The overall feedback applied to (8) is given by

$$u(x) \;\; := \;\; (L_g L_f h(x))^{-1} \cdot \left(\Psi(h(x), L_f h(x)) - L_f^2 h(x) \right). \tag{21}$$

This is the method of computed torque with a finite-time stabilizing controller on each of the double integrators.

IV. Simulations

Consider the biped robot model (8) with the following parameter values (see Figures 4, 5)

Mechanical parameters	Torso	Femur	Tibia
Mass(kg)	M_T=20	M_3=6.8	M_4=3.2
Length (m)	L_T=0.625	L_3=0.4	L_4=0.4
Position of the Center of Mass (m)	X_T=0.01, Z_T=0.2	z_3=0.16	z_4=0.128

[3]The theory in [11], [12] does NOT allow the use a discontinuous feedback as is commonly used in sliding mode control.

Consider the feedback of Section III-B with the following parameters[4]

Output	Gain	Parameters
y_1	k_1=62.5	$q_{1d} = \pi/30$ rad
y_2	k_2=500	
y_3	k_3=1	$z_{H\text{MIN}} = 0.745\ m$, $z_{H\text{MAX}} = 0.76\ m$, sld= $0.5\ m$
y_4	k_4=1	$z_{2\text{MAX}} = 0.01\ m$, sld= $0.5\ m$

The initial velocity of the hips, v_H^-, equals 1.25 m/s. In the feedback (21), $\epsilon = 0.05$ and $\alpha = 0.9$. The parameter $\epsilon > 0$ allows the settling time of the controller to be adjusted and $0 < \alpha < 1$ achieves a finite-settling time. The choice of the parameter values has been made with an eye towards keeping the magnitudes of the applied torques within the capabilities of the actuators of the prototype.

Several aspects of the solution corresponding to the model and feedback with the above parameters are now highlighted. Figure 6 displays the outputs driven to zero by the feedback controller before impact. This implies that the posture constraint encoded in the output function (14) is satisfied and that the proof of stability to be presented in the next section can be applied. Figure 7 displays the walking motion of the biped robot as a series of stick figures over four steps. The walking appears to be natural, i.e., how a human without arms might walk. Figure 8 displays the applied torques over a few walking cycles; note that the peak torque magnitude is about 105 Nm, which is compatible with the prototype RABBIT's torque limits. Figure 9 displays the normal and tangential forces acting on the stance leg end; note that the maximum force is about 700 N, which is compatible with the prototype RABBIT's limit of 1500 N. Figure 10 displays the coordinates z_2 (vertical height of the end of the swing leg) and z_H (vertical height of the hips), which are key quantities in the definition of the outputs used to generate the feedback controller.

In Figures 6–10 the walking trajectories appear to be asymptotically stable. This appearance will be proven in the next section. The feedback parameters chosen in the above table were tuned by hand; a more systematic approach will be presented in a future publication. There is robustness about the choice of feedback parameters; that is, the robot still walks with moderate variations in feedback parameters. The output function chosen, (14), is certainly not unique; for example, controlling torso angle, horizontal hip placement, and swing and stance leg knee angles will also yield a stable walking motion.

[4]The torso appears to be leaning backwards because the center of mass is not located along the axis of the torso.

V. Stability Proof

The purpose of this section is to prove the asymptotic stability or instability of trajectories resulting from the biped in closed loop with the controller (21). An important result from [12] is that stability (or instability) can be proven on the basis of the restriction of the Poincaré map to a one dimensional manifold. In the following, only the bare minimum of mathematical notation needed to use this tool will be introduced. The reader seeking a careful development of these ideas is refereed to [12]. Let Z denote the zero dynamics manifold, i.e. $Z = \{(q, \dot{q}) \in \mathcal{X} | h(q) = 0, L_f h(q) = 0\}$. The conditions required to define the reduced Poincaré map are

1. $S \cap Z$ is a smooth submanifold of $\mathcal{X}$;
2. the decoupling matrix $L_g L_f h$ is invertible; and
3. the convergence time of the controller is strictly less than the time of a single step of the robot.

A. Smoothness of $S \cap Z$

From standard results in [3], $S \cap Z$ will be a smooth one-dimensional manifold if the map

$$\begin{bmatrix} h(q) \\ L_f h(q, \dot{q}) \\ z_2(q) \end{bmatrix} \tag{22}$$

has constant rank[5] equal to nine on $S \cap Z$. A simple argument shows that this is equivalent to the rank of $[h(q)' \; z_2(q)]'$ being equal to five. Hence, define the 5×5 matrix

$$A \;=\; \begin{bmatrix} \frac{\partial h}{\partial q} \\ \frac{\partial z_2}{\partial q} \end{bmatrix} \tag{23}$$

whose determinant in the p coordinates is proportional to

$$\sin(p_{42}) \cdot \sin(p_{31}) \cdot \sin\left(\frac{p_{41}}{2}\right) \cdot \sin(p_{41}). \tag{24}$$

On M, it is easily verified that the determinant vanishes only at $p_{31} = \pi$. However, if $q \in Z$ and $p_{31} = \pi$, then $z_2(q) = 0.01 \neq 0$, and thus $q \notin S$. Hence, the determinant of A is non-zero on $S \cap Z$. If $(q, \omega) \in S \cap Z$, then it follows that q is equal to a constant; call this value q_0. Furthermore, it follows that ω is parameterized by a single variable. This parameterization is developed next. Let

$$\Phi(q) \;=\; \begin{bmatrix} h(q) \\ x_H(q) \end{bmatrix}, \tag{25}$$

[5]Recall that the rank of a map at a point is by definition the rank of its Jacobian matrix evaluated at the same point.

where x_H is the horizontal position of the robot's hips. It is straightforward to verify that Φ has full rank at q_0. On Z, it follows that $\frac{d}{dt}h(q) = L_f h(q,\omega) = 0$, and thus

$$\begin{bmatrix} 0 \\ v_H \end{bmatrix} = \frac{d}{dt}\Phi(q) = \frac{\partial \Phi}{\partial q} \cdot \omega. \tag{26}$$

Thus, $\sigma : I\!R \to S \cap Z$ by

$$\sigma(v_H^-) := \begin{bmatrix} q_0 \\ \left[\frac{\partial \Phi(q_0)}{\partial q}\right]^{-1} \cdot v_H^- \end{bmatrix} \tag{27}$$

is a diffeomorphism from $I\!R$ to $S \cap Z$, with v_H^- the hips horizontal velocity just before the impact.

B. Proof of the decoupling matrix invertibility

The complexity of the decoupling matrix, $L_g L_f h$, makes a direct proof of invertibility highly non-trivial. Moreover, since the point $q_{ext} = (\pi, \pi, \pi, \pi, 0)'$ is an extremum of the height of the hips, the decoupling matrix for the choice of outputs (14) is necessarily singular at q_{ext}. Hence, proof of the invertibility of the decoupling matrix must be local in q. One method of local proof is to demonstrate sign definiteness of the decoupling matrix's determinant in an open set about the biped's trajectories. Sign definiteness implies the determinate never equals zero in that set and, hence, in that set, the decoupling matrix is invertible. This is the method used here. The proof is carried out in two steps. In the first step, the decoupling matrix is simplified by the application of an invertible feedback [22] to the model[6]. In the second step, elementary bounds on the individual terms appearing in the determinant of the decoupling matrix are determined and used to compute upper and lower bounds on the determinant of the decoupling matrix. To apply the technique of [22], it is easiest to work in relative coordinates

$$\bar{q} := (\bar{q}_{31}, \bar{q}_{41}, \bar{q}_{32}, \bar{q}_{42}, q_1)' \tag{28}$$

where

$$\begin{bmatrix} \bar{q}_{31} \\ \bar{q}_{41} \\ \bar{q}_{32} \\ \bar{q}_{42} \end{bmatrix} = \begin{bmatrix} q_{31} - q_1 \\ q_{31} - q_{41} \\ q_{32} - q_1 \\ q_{32} - q_{42} \end{bmatrix}. \tag{29}$$

Denote the dynamic model (1) in these new coordinates as

$$\bar{D}(\bar{q}) \cdot \ddot{\bar{q}} + \bar{C}(\bar{q}, \dot{\bar{q}}) \cdot \dot{\bar{q}} + \bar{G}(\bar{q}) \;\; = \;\; \bar{B} \cdot u. \tag{30}$$

[6]By standard results in [16], the invertibility of the decoupling matrix is invariant under the application of invertible feedbacks.

It is easily shown that $\bar{B}$ has the form

$$\bar{B} = \begin{bmatrix} I \\ 0 \end{bmatrix}. \tag{31}$$

Next, partition the coordinates into

$$q_a = (\bar{q}_{31}, \bar{q}_{41}, \bar{q}_{32}, \bar{q}_{42})' \quad \text{and} \quad q_b = q_1, \tag{32}$$

the "actuated" coordinates and "un-actuated" coordinates, respectively. Write (30) as

$$\bar{D}_{11}(\bar{q})\ddot{q}_a + \bar{D}_{12}(\bar{q})\ddot{q}_b + \bar{C}_1(\bar{q},\dot{\bar{q}})\dot{q}_a + \bar{G}_1(\bar{q}) = u \tag{33}$$

$$\bar{D}_{21}(\bar{q})\ddot{q}_a + \bar{D}_{22}(\bar{q})\ddot{q}_b + \bar{C}_2(\bar{q},\dot{\bar{q}})\dot{q}_a + \bar{G}_2(\bar{q}) = 0, \tag{34}$$

and solve (34) for $\ddot{q}_b$ as

$$\ddot{q}_b = -\bar{D}_{22}(\bar{q})^{-1}\left(\bar{D}_{21}(\bar{q})\ddot{q}_a + \bar{C}_2(\bar{q},\dot{\bar{q}})\dot{q}_a + \bar{G}_2(\bar{q})\right). \tag{35}$$

Substituting (35) into (33) yields

$$\hat{D}(\bar{q})\ddot{q}_a + \hat{C}(\bar{q},\dot{\bar{q}})\dot{q}_a + \hat{G}(\bar{q}) = u \tag{36}$$

where[7]

$$\hat{D}(\bar{q}) = \bar{D}_{11}(\bar{q}) - \bar{D}_{12}(\bar{q})\bar{D}_{22}^{-1}(\bar{q})\bar{D}_{21}(\bar{q}) \tag{37}$$

$$\hat{C}(\bar{q},\dot{\bar{q}}) = \bar{C}_1(\bar{q},\dot{\bar{q}}) - \bar{D}_{12}(\bar{q})\bar{D}_{22}^{-1}(\bar{q})\bar{C}_2(\bar{q},\dot{\bar{q}}) \tag{38}$$

$$\hat{G}(\bar{q}) = \bar{G}_1(\bar{q}) - \bar{D}_{12}(\bar{q})\bar{D}_{22}^{-1}(\bar{q})\bar{G}_2(\bar{q}). \tag{39}$$

Applying the partial linearizing feedback

$$u = \hat{D}(\bar{q})v + \hat{C}(\bar{q},\dot{\bar{q}})\dot{q}_a + \hat{G}(\bar{q}) \tag{40}$$

to (33) allows (33) and (34) to be re-written as

$$\ddot{q}_a = v \tag{41}$$

$$\ddot{q}_b = -\bar{D}_{22}(\bar{q})^{-1}\left(\bar{D}_{21}(\bar{q})\ddot{q}_a + \bar{C}_2(\bar{q},\dot{\bar{q}})\dot{q}_a + \bar{G}_2(\bar{q})\right). \tag{42}$$

The model (41) and (42) is feedback equivalent to the original system. It can be expressed in state space form with the same choice of x as before to obtain

$$\dot{x} = \hat{f}(x) + \hat{g}(x)v. \tag{43}$$

[7]The invertibility of $\bar{D}_{22}$ is assured by the positive definiteness of D.

Since the rank of the decoupling matrix is invariant under invertible feedback, the decoupling matrices for systems (2) and (43) have the same rank. The determinant of the decoupling matrix for (43) can be directly computed and shown to be of the form[8]

$$\det L_{\hat{g}} L_{\hat{f}} h(\bar{q}) = \frac{\mathrm{Num}(\bar{q})}{\mathrm{Den}(\bar{q})} \tag{44}$$

with

$$\mathrm{Num}(\bar{q}) = \sum_{i=1}^{114} k_i^N g_i^N \left(c_i^N \bar{q}\right) \quad \text{and} \quad \mathrm{Den}(\bar{q}) = \sum_{i=1}^{11} k_i^D g_i^D \left(c_i^D \bar{q}\right) \tag{45}$$

where the k_i's are constants, g_i's are sine and cosine functions, and c_i's are row vectors in $\mathbb{R}^5$. For a given subset $\mathcal{O} \subset M$ (recall that M is the allowed set for the configuration variables), upper and lower bounds on the determinant of the decoupling matrix can be found via calculation of the minimum and maximum of each of the 125 terms of the numerator and denominator over $\mathcal{O}$. For example, if the denominator in (44) is positive, then

$$\max_{\bar{q}\in\mathcal{O}} \det L_{\hat{g}} L_{\hat{f}} h(\bar{q}) \leq \frac{\max_{\bar{q}\in\mathcal{O}} \mathrm{Num}(\bar{q})}{\min_{\bar{q}\in\mathcal{O}} \mathrm{Den}(\bar{q})} \leq \frac{\max_{i\in I} \max_{\bar{q}\in\mathcal{O}_i} \mathrm{Num}(\bar{q})}{\min_{i\in I} \min_{\bar{q}\in\mathcal{O}_i} \mathrm{Den}(\bar{q})}, \tag{46}$$

where, $\mathcal{O} \subset \bigcup_{i\in I} \mathcal{O}_i$, and the $\mathcal{O}_i$ are closed and bounded. The max and min operations in (46) are especially trivial to evaluate if the sets $\mathcal{O}_i$ are selected to be of the form

$$\begin{aligned} \mathcal{O}_i := \Big\{ x \mid\ & \bar{q}_{31,i}^{min} \leq \bar{q}_{31} \leq \bar{q}_{31,i}^{max},\ \bar{q}_{41,i}^{min} \leq \bar{q}_{41} \leq \bar{q}_{41,i}^{max}, \\ & \bar{q}_{32,i}^{min} \leq \bar{q}_{32} \leq \bar{q}_{32,i}^{max},\ \bar{q}_{42,i}^{min} \leq \bar{q}_{42} \leq \bar{q}_{42,i}^{max}, q_{1,i}^{min} \leq q_1 \leq q_{1,i}^{max} \Big\}. \end{aligned} \tag{47}$$

The above technique was applied to the apparent limit-cycle of Section of IV. Individual closed sets $\mathcal{O}_i$ were determined by dividing the time trajectory into disjoint pieces, and over bounding the configuration variables so that over the $i-th$ time interval, the trajectory of the configuration variables lies strictly in the interior of $\mathcal{O}_i$. As an illustration, Figure 13 shows the result of this process for $\bar{q}_{31}$. Division of the trajectories in time into pieces over which the determinant could be proven to be sign definite was accomplished with a simple binary search algorithm. The results of this process are presented in Table I, which gives the upper and lower bounds of the determinant of the decoupling matrix as well as the minimum and maximum of the determinant over each subset, and the beginning and end of each set's division in time. It should be noted that: (1) this process could be iterated to prove the decoupling matrix's invertibility over a larger subset of the biped's state space, and, (2) the

[8]It is straightforward to check that the decoupling matrix depends only upon the configuration variables, q, and not on the angular velocities.

fact that this method works is not an accident. Results from real analysis can be used to show that the decoupling matrix is invertible on an open set about the configuration variable trajectories if and only if a there exists a set $\mathcal{O}$ which is the interior of a union of a *finite* number of closed sets $\mathcal{O}_i$ as described above.

C. The reduced Poincaré map

The Poincaré surface will be taken to be S, the impact surface. Let $P : S \to S$ be the usual Poincaré[9] map. For those trajectories for which the convergence time of the controller (21) is less than the time to make a single step, the trajectory will have converged to the zero dynamics manifold, Z, in finite-time. In this case, P takes values in $S \cap Z$. The *reduced Poincaré map* is defined to be $\rho : S \cap Z \to S \cap Z$ by $\rho(x) = P(x)$; that is $\rho := P|_{S\cap Z}$. To compute ρ, it is easiest to use the identification of $S \cap Z$ with $\mathbb{R}$ given by (27). Thus, define $\lambda : \mathbb{R} \to \mathbb{R}$ by $\lambda := \sigma^{-1} \circ \rho \circ \sigma$. The function λ can be computed in a straightforward manner:

Reduced Poincaré map: $\lambda : \mathbb{R} \to \mathbb{R}$

1. Let $v_H^- > 0$ denote the horizontal velocity of the robot's hips just before impact (the restriction to positive velocities corresponds to the robot walking from left to right). Compute $x^- := \sigma(v_H^-) \in S \cap Z$, the position of the robot just before impact.

2. Apply the impact model to x^-, that is, compute $x^+ := \Delta(x^-)$.

3. Use x^+ as the initial condition in (2) controlled by (21), the robot in closed loop with the controller, and simulate until one of the following happens:

a. There exists a (first) time $T > 0$ where $z_2(T) = 0$. If T is greater than the settling time of the controller, then $\lambda(v_H^-) := v_H^+(T)$; else, $\lambda(v_H^-)$ is undefined at this point.

b. There does not exist a $T > 0$ such that $z_2(T) = 0$; in this case, it is also true that $\lambda(v_H^-)$ is undefined at this point. ■

D. Stability results

To determine if the closed-loop system is stable under the controller (21), the function λ is computed for $v_H^- \in [1, 2]$. Figure 11 displays the functions λ. One deduces that λ is undefined for v_H^- less than

[9]Since not every initial condition in S will result in the robot making a successful step, P is in general only a partial map; that is, its domain of definition is not all of S. The same is true, of course, for the reduced Poincaré map.

1.05 m/s and more than 1.55 m/s. A fixed point appears at approximately 1.25 m/s, and corresponds to an asymptotically stable walking cycle. Figure 12 displays the limit cycle over several steps with the previous parameters of simulation, in particular $v_H^- = 1.25\ m/s$; it appears that the trajectory is very close to the limit cycle at the beginning of the simulation, which confirms that the point $v_H^- = 1.25\ m/s$ is fixed.

VI. Walking on a Compliant Surface

On the actual prototype, the contact between the ends of the legs and the ground will not be rigid and the ends of the legs may slip. This section presents the results of evaluating the controller (21) on a detailed simulator for RABBIT [28] that includes the normal forces on the legs due to a compliant contact with the ground [14], [20], [5] and the tangential forces due to dynamic friction [4], [19], [23]. For the sake of completeness, the models are first summarized and then the simulation results are reported.

The rigid and compliant models are conceptually very different. As presented in Section II, the rigid model is composed of a dynamical nonlinear system for the swing phase, and an impulsional system for the contact event. With the assumptions stated in Section II (in particular, the impact is instantaneous), this implies that there is no double support phase during a step. The compliant model, on the other hand, is an ordinary (non-hybrid) dynamical nonlinear system and allows a double support phase where there is simultaneous contact between the swing leg and the ground and the stance leg and the ground. Of course, this fact was not taken into account in the synthesis of the controller, and applying the controller to the case of walking on a compliant surface allows a check of its robustness properties.

A. Compliant contact and friction models

The dynamic model is based on the full 7 DOF model of the biped with a computation of the forces acting on the end of each leg:

$$D_e(q_e) \cdot \ddot{q_e} + C_e(q_e, \dot{q_e}) \cdot \dot{q_e} + G_e(q_e) \quad = \quad B_e \cdot u + J_e'(q_e) \cdot F, \tag{48}$$

where, $q_e = (q_{31}, q_{32}, q_{41}, q_{42}, q_1, x_H, z_H)'$, $J(q_e)$ is the 4×7 Jacobian matrix of the end points of the two legs

$$J_e(q_e) = \frac{\partial}{\partial q_e} \begin{bmatrix} x_1(q_e) \\ z_1(q_e) \\ x_2(q_e) \\ z_2(q_e) \end{bmatrix}, \tag{49}$$

and F consists of the normal and tangential forces acting on the ends of the two legs

$$F = (F_{n1}, F_{t1}, F_{n2}, F_{t2})'. \tag{50}$$

The robot's dynamics are then described by ordinary (non-hybrid) differential equations over the entire step, even during the impact, which will have a non-zero duration. The model of the normal force can be viewed as a vertical nonlinear spring-damper. Let z_G be the penetration of a link into the ground, λ_v the damping coefficient of the vertical damper, k_v the stiffness of the vertical spring and n a coefficient characterizing the form of the surfaces in contact. Note, if $z_G > 0$, the link is not touching the ground, then these forces are equal to zero.

The normal force applied to the link when in contact with the ground is given by

$$F_n = -\lambda_v \cdot |z_G|^n \cdot \dot{z}_G + k \cdot |z_G|^n. \tag{51}$$

The tangential force, $F_t = \mu(d, v) \cdot |F_n|$, is in the form of a friction model with a non-constant coefficient of friction. The *Lugre* friction model is used to evaluate the friction coefficient μ [4], [23]. This model supposes that the interface between the two contacting surfaces is a contact between bristles. The bristle dynamics are modeled by horizontal springs and dampers, which, if the applied tangential force is sufficient, are deflecting and slipping. The model uses the average deflection d of the bristles as the internal state of the friction, $\dot{d} = v - |v| \cdot \frac{\sigma_{h0}}{\alpha_{h0}} \cdot d$, where v is the relative velocity of the contacting surfaces, σ_{h0} the stiffness of the horizontal spring and α_{h0} is the coefficient of static friction. In the overall friction coefficient, $\mu(d) = \sigma_{h0} \cdot d + \sigma_{h1} \cdot \dot{d} + \alpha_{h2} \cdot v$, σ_{h1} is the damping coefficient of the horizontal damper and α_{h2} is the coefficient of viscous friction. Thus, the complete model of the tangential force is given by

$$\begin{aligned} F_t &= \mu(d) \cdot |F_n| \\ \dot{d} &= v - |v| \cdot \frac{\sigma_{h0}}{\alpha_{h0}} \cdot d \\ \mu(d, v) &= \sigma_{h0} \cdot d + \sigma_{h1} \cdot \dot{d} + \alpha_{h2} \cdot v \end{aligned} \tag{52}$$

In the case of the biped, the above models are applied to the ends of each of the legs. The penetration z_{Gi} (where i equals 1 or 2) is the vertical coordinate of the end of leg i; this value is derived from the height of the hips, z_H, and the angular coordinates q_{3i} and q_{4i}

$$z_{Gi} = z_H + L_3 \cdot \cos(q_{3i}) + L_4 \cdot \cos(q_{4i}) \tag{53}$$

The relative velocity v_i (where i equals 1 or 2) is the relative velocity of the end of the leg i with respect to the ground; this value is derived from the horizontal velocity of the hips $\dot{x}_H$, and the angular coordinates and velocities q_{3i}, q_{4i}, $\dot{q}_{3i}$ and $\dot{q}_{4i}$

$$v_i = \dot{x}_H - L_3 \cdot \cos(q_{3i}) \cdot \dot{q}_{3i} - L_4 \cdot \cos(q_{4i}) \cdot \dot{q}_{4i} \tag{54}$$

B. Simulations

In this section, the feedback controller of Section III-B is directly applied to the biped robot model derived from (48). It is assumed that the mechanical parameters defined in Section IV are the same, and that the parameters of the controller have not been changed. The initial condition v_H^- is started at 1.25 m/s, i.e. the same initial condition used in the rigid case. The ground parameters are taken to be as close as possible to the parameters of the ground used by the prototype RABBIT

$$\begin{array}{llll} \lambda_v = 6 \times 10^6, & n = 1.5, & k = 20 \times 10^6, & \\ \sigma_{h0} = 260, & \sigma_{h1} = 0.6, & \alpha_{h0} = 0.285, & \alpha_{h2} = 0.18. \end{array} \tag{55}$$

Note that

1. $n = 1.5$ since the end of each of RABBIT's legs is equipped with a wheel in the frontal plane,

2. The walking surface for the prototype RABBIT is quite rigid as can be seen by the stiffness k_v and the damping coefficient λ_v.

The controller in closed-loop with the 7 DOF robot model and the compliant contact model still results in an apparently attractive limit cycle. Figures 14-18 present some simulation results over a few cycles near the stable orbit. Figure 14 displays the outputs, which are still driven to zero before the impact. The walking motion of the biped robot is shown in Figure 15 over four steps; the average walking speed of the robot on the compliant surface is very close to the walking speed under the rigid contact model, 0.75 m/s. Figure 16 displays the applied torques over a few walking cycles (four steps); note that the peak torque magnitude is now around 100 Nm, or about 5 Nm less than in the rigid case. Figure 17

displays the normal forces acting on the leg ends: it is clear that there is now a double-support phase. One cannot directly compare the forces with the rigid case where the forces due to the impact were modeled as impulses. Figure 18 displays the coordinates z_H, z_1 and z_2, which give the vertical position of the hips and the ends of the legs. The coordinate of the end of the stance leg, z_1, is less than zero, showing that there is penetration in the ground of about 0.7 mm, which gives a maximum value of 9.3 mm for z_2.

The model was also simulated with a set of parameters for the contact model, resulting in the stance leg penetrating approximately 15.0 mm into the ground. When the robot was commanded to increase the height of the swing leg by the appropriate amount, stable walking was also achieved, though with a higher average walking speed.

In summary, these results show that the analysis based on a rigid walking model is a good predictor of the robot's behavior on a compliant walking surface, in the case where the "real" walking surface is not too elastic. This gives us the confidence to proceed with the next phase of the project, which is the implementation of the controller on the prototype.

Acknowledgments

The work of J.W. Grizzle and E. Westervelt was supported in part by NSF grants INT-9980227 and IIS-9988695, and in part by the University of Michigan Center for Biomedical Engineering Research (CBER). F. Plestan and G. Abba thank the French Research Group, *Groupe de Recherche Commande de Robots à Pattes*.

References

[1] Bainov, D.D., and Simeonov, P.S., *Systems with impulse effects: stability, theory and applications*, Ellis Horwood Limited, Chichester, 1989.

[2] Bhat, S.P., and Bernstein, D.S., "Continuous finite-time stabilization of the translational and rotational double integrators", *IEEE Trans. Autom. Control*, 43, 5, pp.678-682, 1998.

[3] Boothby, W.M., *An Introduction to Differentiable Manifolds and Riemannian Geometry*, Academic Press, New York, 1975.

[4] Canudas, C., Olsson, H., Aström, K.J., and Lischinsky, P., "A new-model for control of systems with friction", *IEEE Trans. Autom. Control*, 40, 3, pp.419-425, 1995.

[5] Canudas, C., Roussel, L., and Goswani, A., "Periodic stabilization of a 1-DOF hopping robot on nonlinear compliant surface", *Proc. IFAC Symposium on Robot Control*, Nantes, France, September, 1997.

[6] Chevallereau, C., and Sardain, P., "Design and actuation optimization of a 4-axes biped robot for walking and running ", *Proc. IEEE International Conference on Robotics and Automation*, San-Francisco, California, April, 2000.

[7] Eng, J. J., Winter,D. A. and Patla, A. E. "Strategies for recovery from a trip in early and late swing during human walking," *Experimental Brain Research*, 102(2):339–349, 1994.

[8] Eng, J. J., Winter,D. A. and Patla, A. E., "Intralimb dynamics simplify reactive control strategies during locomotion," *Journal of Biomechanics*, 30(5):581–588, June 1997.

[9] François, C., and Samson, C., "A new approach to the control of the planar one-legged hopper", *The International Journal of Robotics Research*, 17, 11, pp. 1150-1166, 1998.

[10] Goswani, A., Espiau, B., and Keramane, A., "Limit cycles and their stability in a passive bipedal gait", *Proc. IEEE International Conference on Robotics and Automation*, Minneapolis, Minnesota, April, 1996.

[11] Grizzle, J.W., Abba, G., and Plestan, F., "Asymptotically stable walking for biped robots: analysis via systems with impulse effects", *IEEE Trans. Autom. Control*, 46, 1, pp. 51-64, 2001.
[12] Grizzle, J.W., Abba, G., and Plestan, F., "Proving asymptotic stability of a walking cycle for a five DOF biped robot model", *Proc. International Conference on Climbing and Walking Robots*, Portsmouth, England, 1999.
[13] J. Guckenheimer and P. Holmes, *Nonlinear Oscillations, Dynamical Systems, and Bifurcations of Vector Fields*, volume 42 of *Applied Mathematical Sciences*. Springer-Verlag, New York, corrected second printing edition, 1996.
[14] Hunt, K.H., and Crosseley, F.R., "Coefficient of restitution interpreted as damping in vibroimpact", *Journal of Applied Mechanics*, pp. 440-445, 1975.
[15] Hurmuzlu, Y., and Marghitu, D.B., "Rigid body collisions of planar kinematic chains with multiple contact points", *The International Journal of Robotics Research*, 13, 1, pp. 82-92, 1994.
[16] Isidori, A., *Nonlinear control systems: an Introduction*, Springer-Verlag, Berlin, 2nd edition, 1989.
[17] Koditschek, D.D., and Buhler, M., "Analysis of a simplified hopping robot", *The International Journal of Robotics Research*, 10, 6, pp. 587-605, 1991.
[18] Kuo, A. D., "Stabilization of lateral motion in passive dynamic walking," *The International Journal of Robotics Research*, 18(9):917–930, 1999.
[19] Lischinsky, P.A., *Compensation de frottement et commande en position d'un robot hydraulique industriel*, Ph.D. Thesis, Institut National Polytechnique de Grenoble, in French, 1997.
[20] Marhefka, D.W., and Orin, D.E., "Simulation of contact using a nonlinear damping model", *Proc. IEEE International Conference on Robotics and Automation*, Mineapolis, Minnesota, April, 1996.
[21] Parker, T.S. and Chua,L.O., *Practical Numerical Algorithms for Chaotic Systems*, Springer-Verlag, New York, 1989.
[22] Reyhanoglu, M., van der Schaft, A., Mcclamroch, N.H., and Kolmanovsky, I., "Dynamics and control of a class of underactuated mechanical systems", *IEEE Transactions on Automatic Control*, 44, 9, pp. 1663-1671, 1999.
[23] Roussel, L., *Génération de trajectoires de marche optimales pour un robot bipède*, Ph.D. Thesis, Institut National Polytechnique de Grenoble, in French, 1998.
[24] Smith, A.C., and Berkemeier, M., "The motion of a finite-width wheel in 3D", *Proc. IEEE International Conference on Robotics and Automation*, Leuven, Belgium, May, 1998.
[25] Spong, M.W., and Vidyasagar, M., *Robot dynamics and control*, John Wiley and Sons, New-York, 1991.
[26] Thuilot, B., Goswani, A., and Espiau, B., "Bifurcation and chaos in a simple passive bipedal gait", *Proc. IEEE International Conference on Robotics and Automation*, Albuquerque, New-Mexico, April, 1997.
[27] Ye, H., Michel, A.N., and Hou, L., "Stability theory for hybrid dynamical systems", *IEEE Trans. Autom. Control*, 43, 4, pp. 461-474, 1998.
[28] www-lag.ensieg.inpg.fr/recherche/cser/PRC-Bipedes/Prototype/rabbit.html.

Set		1	2	3	4	5
$\bar{q}_{31}$	min	200.6015	195.6540	176.6454	168.6733	164.5881
	max	206.2789	204.6540	199.6066	180.2140	172.0809
$\bar{q}_{41}$	min	21.3857	30.2072	31.3540	25.3320	21.3857
	max	30.8175	35.4827	36.7536	31.9875	25.8437
$\bar{q}_{32}$	min	162.5663	167.0718	183.7315	200.8510	201.3176
	max	170.4469	187.4432	204.9086	205.9872	205.9682
$\bar{q}_{42}$	min	18.7285	23.7618	34.4153	26.6624	21.3857
	max	24.2419	38.5711	41.1357	35.1106	27.2010
q_1	min	5.6916	5.7363	5.9273	5.9400	5.9400
	max	6.0600	6.0470	6.0600	6.0600	6.0600
$\det L_{\hat{g}} L_{\hat{f}} h(x)$	min	-310.3236	-529.5476	-631.5226	-422.2026	-266.2791
	max	-0.0245	-0.2840	-0.5837	-0.4718	-3.8473
time	start	0.0000	0.0794	0.2176	0.5539	0.6206
	stop	0.0794	0.2176	0.5539	0.6206	0.6455

TABLE I

$\mathcal{O}$ SET DEFINITION AND DETERMINANT VALUE

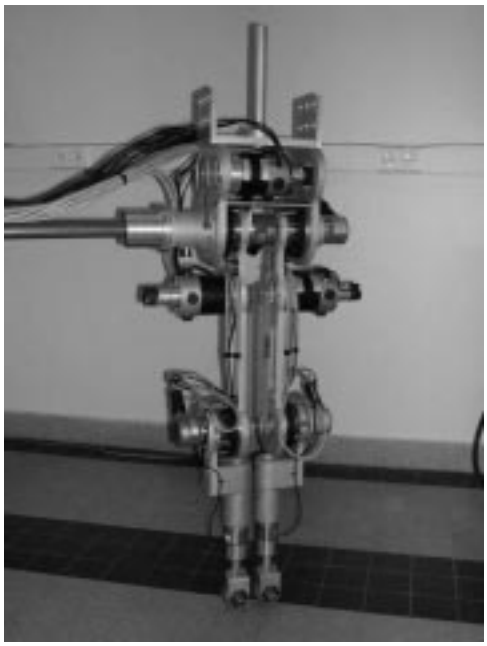

Fig. 1. Photo of RABBIT prototype.

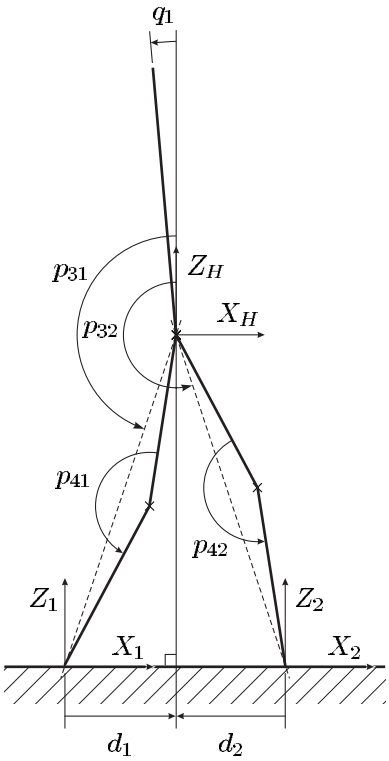

Fig. 3. Schematic of biped robot; relative angles.

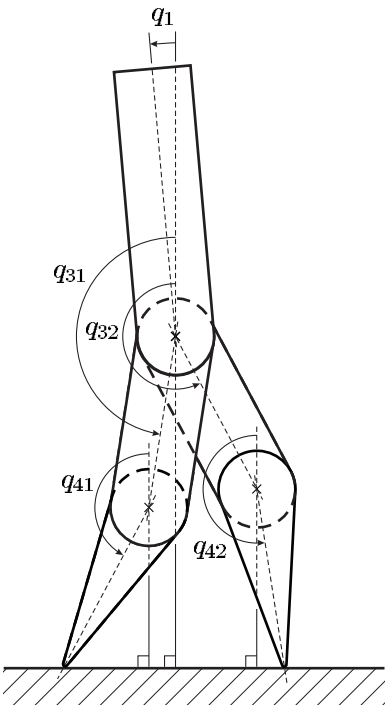

Fig. 2. Schematic of biped robot; absolute angles.

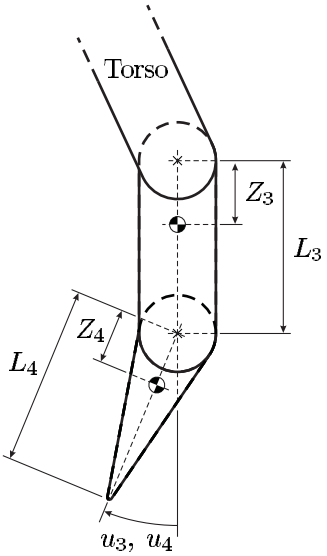

Fig. 4. Schematic of biped robot leg.

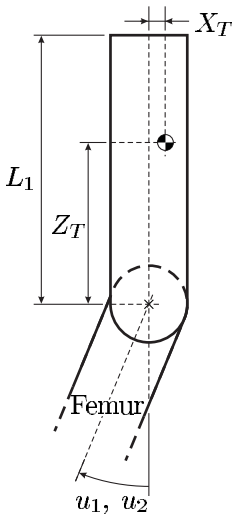

Fig. 5. Schematic of biped robot torso.

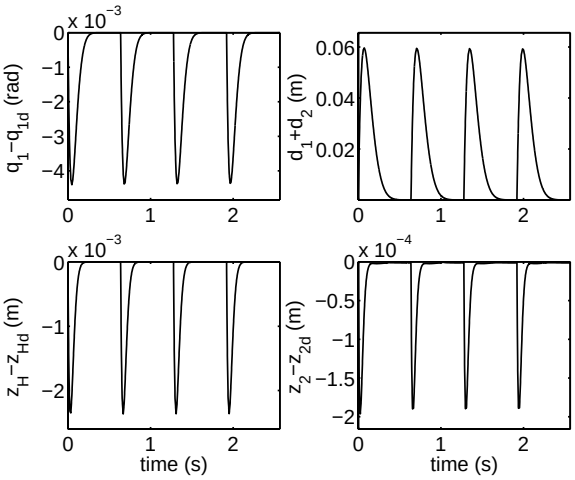

Fig. 6. Plot of outputs used to define the controller versus time. Each output is driven to zero within a single stride.

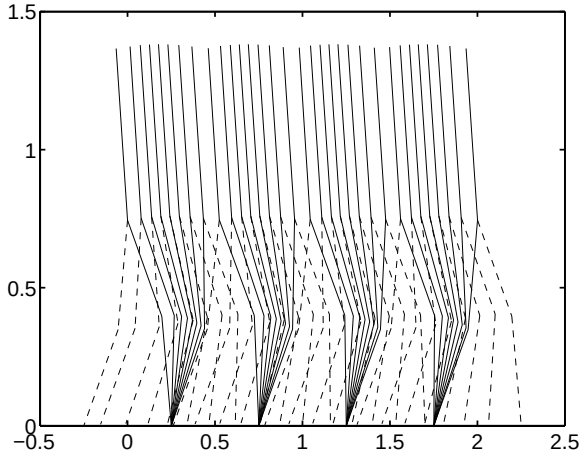

Fig. 7. Plot of walking as a sequence of stick figures; units of meters. The dashed line is the swing leg.

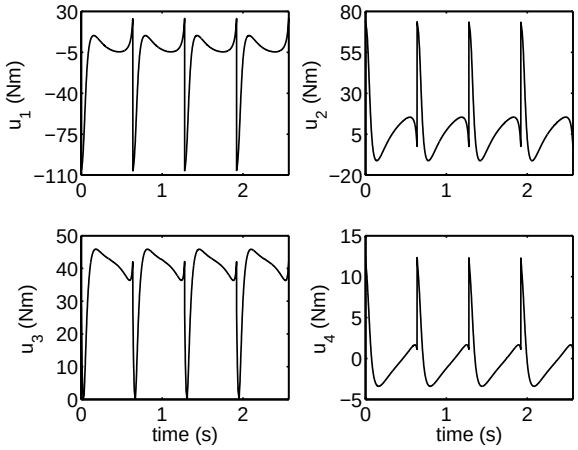

Fig. 8. Plot of applied torques (Newton-meters) versus time.

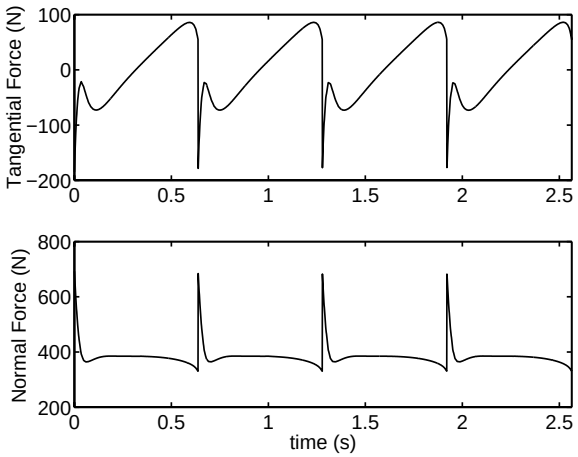

Fig. 9. Plot of normal and tangential forces (Newtons) acting on the stance leg end versus time.

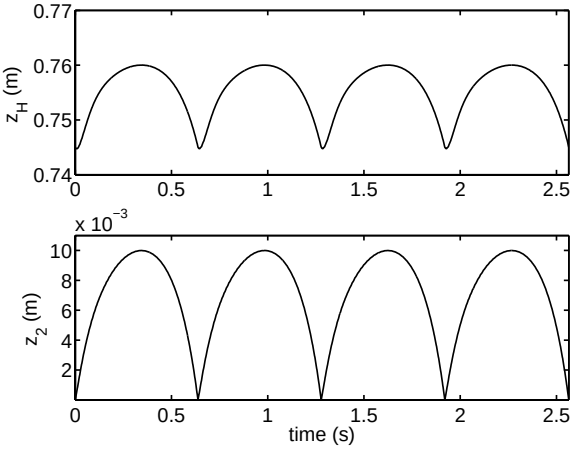

Fig. 10. Plot of z_H and z_2 (meters).

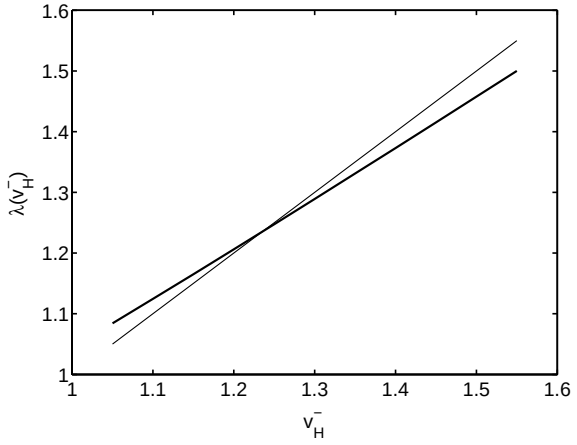

Fig. 11. Function λ (bold line) and identity function (thin line) versus v_H^-. This graph establishes the existence of an asymptotically stable walking motion.

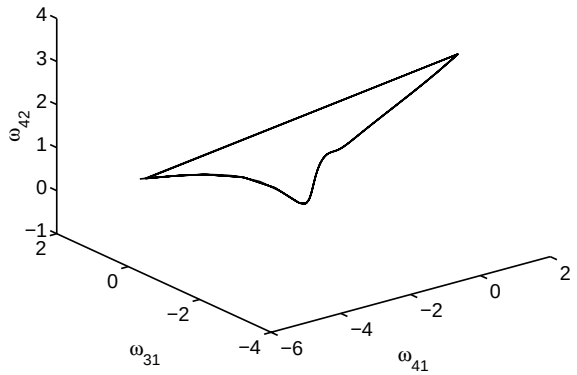

Fig. 12. Three-dimensional projection of the attractive orbit. The straight line portion of the plot in the back top is actually the instantaneous change in velocity at the impact.

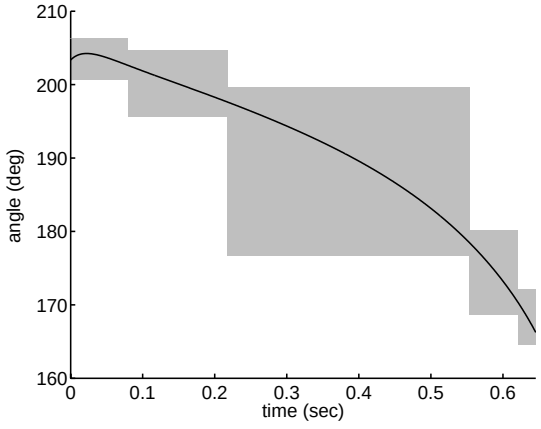

Fig. 13. Projection of the determined subsets $\mathcal{O}_i$ onto the $\bar{q}_{31}$ trajectory. Note that $\bar{q}_{31}(t)$ lies strictly within the union of the interiors of the subsets. The same is true of each of the other configuration variables.

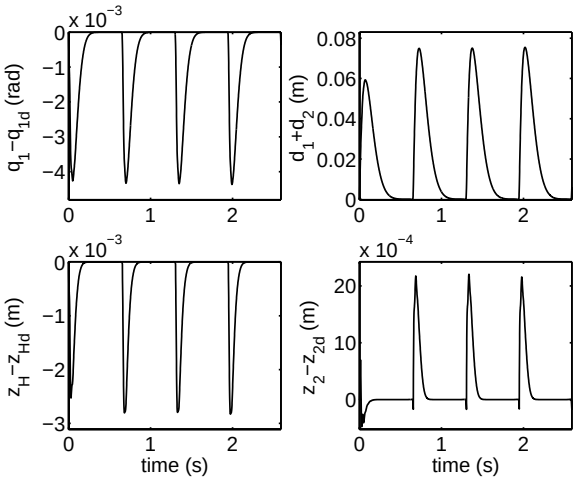

Fig. 14. Plot of outputs used to define the controller versus time for the compliant surface. Each output is almost driven to zero within a single stride.

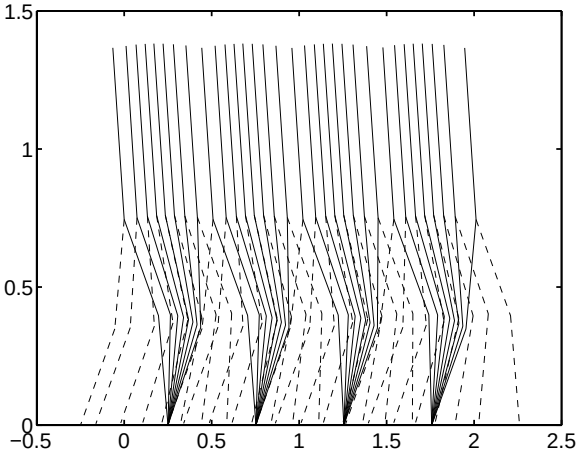

Fig. 15. Plot of walking as a sequence of stick figures for the compliant surface; units of meters. The dashed line is the swing leg.

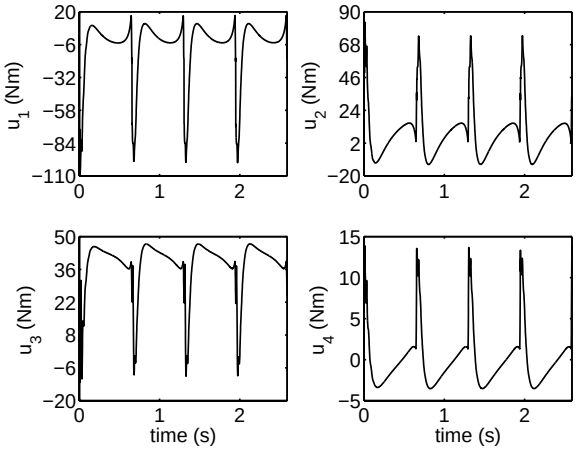

Fig. 16. Plot of applied torques (Newton-meters) versus time for the compliant surface.

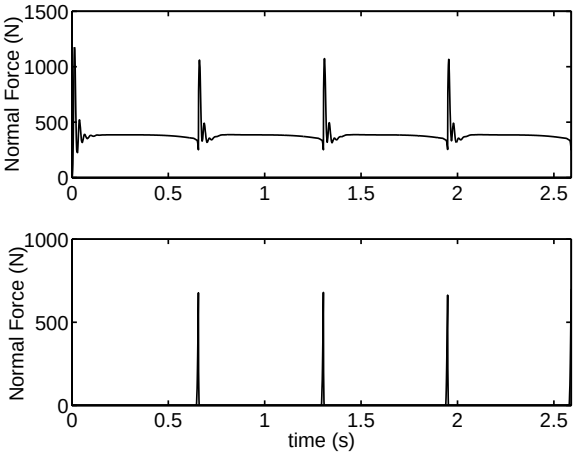

Fig. 17. Plot of normal forces (Newtons) acting on the stance leg (top) and the swing leg (bottom) ends versus time for the compliant surface.

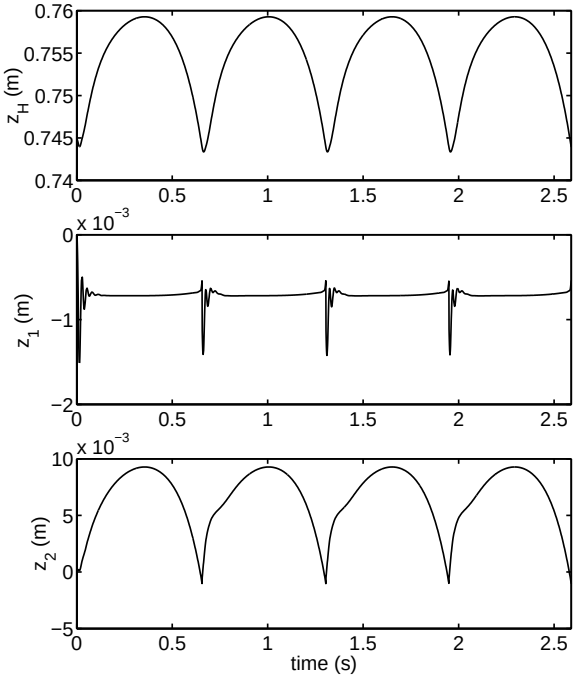

Fig. 18. Plots of z_H, z_1 and z_2 (meters) for the compliant surface.